Colloids and Surfaces A: Physicochem. Eng. Aspects 497 (2016) 316–326

Contents lists available at ScienceDirect

Colloids and Surfaces A: Physicochemical and Engineering Aspects

journal homepage: www.elsevier.com/locate/colsurfa

Influence of particle shape on the rheological behavior of three-phase non-brownian suspensions

Johannes Maurath*, Boris Bitsch, Yvonne Schwegler, Norbert Willenbacher

Karlsruhe Institute of Technology, Institute for Mechanical Process Engineering and Mechanics, Gotthard-Franz-Strasse 3, 76131 Karlsruhe, Germany

HIGHLIGHTS

- Rheology and structure analysis of three-phase suspensions including anisotropic particles.
- Stable capillary suspensions from spherical and plate-like particles.
- Suspensions of plate-like particles accommodate large amounts of secondary fluid.
- No spherical agglomeration for three-phase suspensions with plate-like particles.
- Versatile basic concept for the design of complex multi-component paste-like products.

GRAPHICAL ABSTRACT

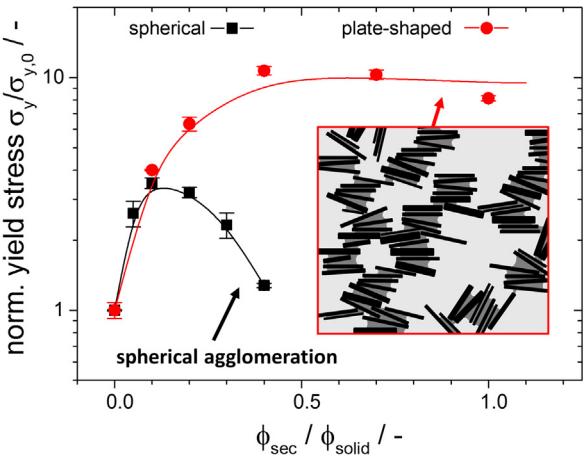

ARTICLE INFO

Article history:
Received 14 December 2015
Received in revised form 2 March 2016
Accepted 3 March 2016
Available online 5 March 2016

Keywords:
Capillary suspensions
Particle shape
Aspect ratio
Microstructure
Rheology
Three-phase suspensions

ABSTRACT

Capillary suspensions are three-phase fluids comprising a solid and two immiscible, liquid phases with unique texture and flow properties. So far, research focused on isometric particles, here we discuss how the addition of a second, immiscible fluid affects structure and flow of suspensions including anisotropic particles. Differently shaped calcium carbonate as well as graphite and aluminum particles have been investigated.

For needle-shaped and scalenohedral particles no increase in yield stress σ_y or storage modulus G' characteristic for a strong capillary force controlled, percolating particle network is observed when a secondary fluid is added. In contrast, a pronounced increase in σ_y and G' is found when a secondary fluid is introduced to suspensions of plate-like particles and optical as well as electron microscopy confirm the formation of a sample-spanning network characteristic for capillary suspensions.

Suspensions of isometric particles exhibit a distinct maximum in σ_y or G' at low fractions of secondary fluid to particle volume fraction $\phi_{sec}/\phi_{solid} \approx 0.1–0.2$, whereas suspensions of plate-like particles exhibit constant σ_y and G' values over a wide range of ϕ_{sec}/ϕ_{solid} values up to ≈ 1 until spherical agglomeration occurs. Due to the different shape of the capillary bridges suspensions of plate-like particles can accommodate much larger fractions of secondary fluid until spherical agglomeration sets in than systems including spherical particles thus offering a versatile basic concept for the design of complex multi-component paste-like products.

* Corresponding author.
E-mail address: johannes.maurath@kit.edu (J. Maurath).

http://dx.doi.org/10.1016/j.colsurfa.2016.03.006
0927-7757/

1. Introduction

Capillary suspensions are three-phase fluids including a solid and two immiscible liquid phases. Addition of a small fraction (typically < 5 vol%) of a secondary liquid phase to a suspension of particles dispersed in the so-called primary or bulk phase leads to the formation of a strong, sample spanning particle network, even at low particle loadings. The particle network gains its strength from the capillary forces inferred from the added secondary liquid no matter whether it wets the particles better or worse than the primary liquid. Generally, non-Brownian particles are employed (particle size varies between 0.5 and 50 μm) and particle loadings range between 5 vol% and 40 vol% [1–5].

Two types of capillary suspensions are distinguished depending on the three-phase wetting angle θ_{SB} the secondary liquid (S) forms against the solid surface in the bulk phase environment (B). In the pendular state ($\theta_{SB} < 90^\circ$), the secondary liquid wets the solid phase better than the bulk fluid and forms pendular bridges between the particles. In the case where $\theta_{SB} > 90^\circ$, termed the capillary state, the particles form clusters around small volumes of the second fluid [5]. Both scenarios finally result in a percolating particle network.

The capillary force F_c between two particles connected by a pendular bridge is composed of two parts: the Laplace pressure inside the bridge and the interfacial tension acting at the solid-liquid–liquid contact line. F_c depends on the diameter x of the particles, their separation distance s, the surface tension of the liquid Γ, as well as the volume V and shape of the liquid bridge. Analytical as well as computational solutions for F_c assume a certain bridge shape (e.g. toroidal, cylindrical, etc.) or solve the Laplace-Young equation directly [2 and references therein]. For a finite particle separation of equally sized spheres connected by a fluid bridge, the capillary force is given by

$$F_c = \frac{x\pi \quad \Gamma \quad \cos\theta_{SB}}{1 + 1.05\hat{s}^2 + 2.5\hat{s}^2}\hat{s} = s\sqrt{\frac{x}{2V}} \tag{1}$$

which simplifies to the well-known expression $F_c = x\pi\Gamma\cos\theta_{SB}$ for spheres that are in contact [6]. The equation for the capillary force may be modified to account for spheres of different sizes [7], rough spheres [8], and changes to bridge volume [9,10]. The typical range for the ubiquitous van der Waals force is on the order of a few nanometers and depletion forces in colloidal systems typically act on the order of 100 nm. In contrast, the capillary force acts on a much longer length scale of typically 10–100 μm and its absolute value is generally orders of magnitude larger than that of the vdW force. The yield stress σ_y of a pendular state suspension similar as for wet granular matter is related to the capillary force [11,12].

$$\sigma_y = f\left(\phi\right) g\left(V, s\right) \frac{\Gamma \quad \cos\theta}{x} \tag{2}$$

where $f(\phi)$ is a function of the particle volume fraction and depends on the number of contacts per particle. The volume of the bridge V and the distance between the two particles s are included in the function g(V,s).

For the capillary state, calculations and experiments have shown that clusters of different shape and structure are formed within the suspension strongly depending on the amount of secondary liquid and its wetting behavior. With higher amounts of secondary liquid, particles tend to form octahedral clusters that have a stronger cohesion than tetrahedral clusters which are more favored for lower secondary liquid contents [5,11,13].

In both, the capillary and the pendular state, capillary suspensions exhibit a unique paste-like texture. They exhibit an apparent yield stress σ_y, gel-like elastic behavior with a high, frequency independent storage modulus G' much larger than the loss modulus G", and a strongly shear thinning flow behavior which renders this class of materials a promising generic formulation platform for a broad variety of applications. Capillary suspensions are highly resistant to sedimentation, and flow properties can be tuned in a wide range to meet different processing or application demands. Even the flow behavior of methane hydrates turned out to be strongly affected by capillary bridging [14]. A broad range of innovative products including novel food formulations, such as heat stable and low calorie chocolate spreads [15,16], capillary suspension based foams [17,18] or pastes for printed electronics, e.g. lithium-ion battery electrodes or front side metallization of solar cells with unique shape accuracy and surface uniformity have been developed [19]. The capillary suspension concept has also been used to control structure formation in particle-laden polymer blends [20] and to assemble metals and nanoparticles into novel nanocomposite superstructures [21]. Beyond that capillary suspensions can be utilized as precursors for highly porous sintering materials to be used as light weight construction materials, filters or membranes [13,22–24].

So far, investigations have been restricted to suspensions including spherical, close-to-spherical or isometric particles. However, understanding capillary phenomena in three-phase suspensions of non-isometric particles is of fundamental academic interest, and beyond that many technically important materials include non-spherical, highly anisotropic particles like fibers or plates. E.g. they are used as pigments in coatings and inks, as fillers in adhesives and sealants or to provide strength to polymeric materials. Also the flow behavior of suspensions of organic matter, like rigid macromolecules (e.g. xanthan, schizophyllan) viruses or coke particles, is of high interest. Accordingly, the rheology of anisotropic, non-Brownian particle suspensions has been explored for a century including experimental, theoretical, and numerical investigations [25–34]. The intrinsic viscosity of differently shaped particles has been calculated [27–29]. Basically, the viscosity at a given volume fraction is higher the more the particle shape differs from a sphere [30], e.g. the higher the aspect ratio r for fibers [31], and prolate, fiber- or needle-like particles yield a higher viscosity than plate- or disk-shaped, oblate particles [30,35]. For concentrated suspensions structural order, particle interactions and number of particle contacts as well as particle orientation and flow-alignment have to be considered and empirical models for the limiting low and high shear viscosity as a function of particle volume fraction have been suggested [30,34]. However, it should be kept in mind the maximum packing fraction for anisotropic particles is higher than for spheres [36]. Complex phase behavior including liquid crystalline structures and arrested states may occur at particle loadings well below maximum packing resulting in complex flow behavior [37,38].

Here we focus on the question how the addition of small amounts of secondary immiscible fluids affects the flow behavior of non-Brownian suspensions including anisotropic particles. We have investigated whether capillary suspensions similar as for spherical particles can be formed, and how their characteristic flow behavior depends on particle shape and secondary fluid content. Precipitated calcium carbonate (PCC) particles with different shape (spherical, scalenohedral, needle-shaped, plate-shaped) have been employed as model systems. Yield stress and storage modulus have been measured since these quantities are very sensitive to structural changes. Confocal laser scanning microscopy (CLSM) and scanning electron microscopy (SEM) have been utilized to visualize the suspension microstructure in the wet and in the solid state. In addition, two material systems potentially relevant for printed electronic applications or energy storage and conversion systems have been investigated, namely aluminum flake suspensions with different diameter to width ratio and graphite suspensions based on particles with spherical and oblate shape. For such applications conductivity in the final dry film is a key feature and is supposed to be higher using oblate instead of spherical particles [39,40]. The capillary suspension based formulation concept is of special rele-

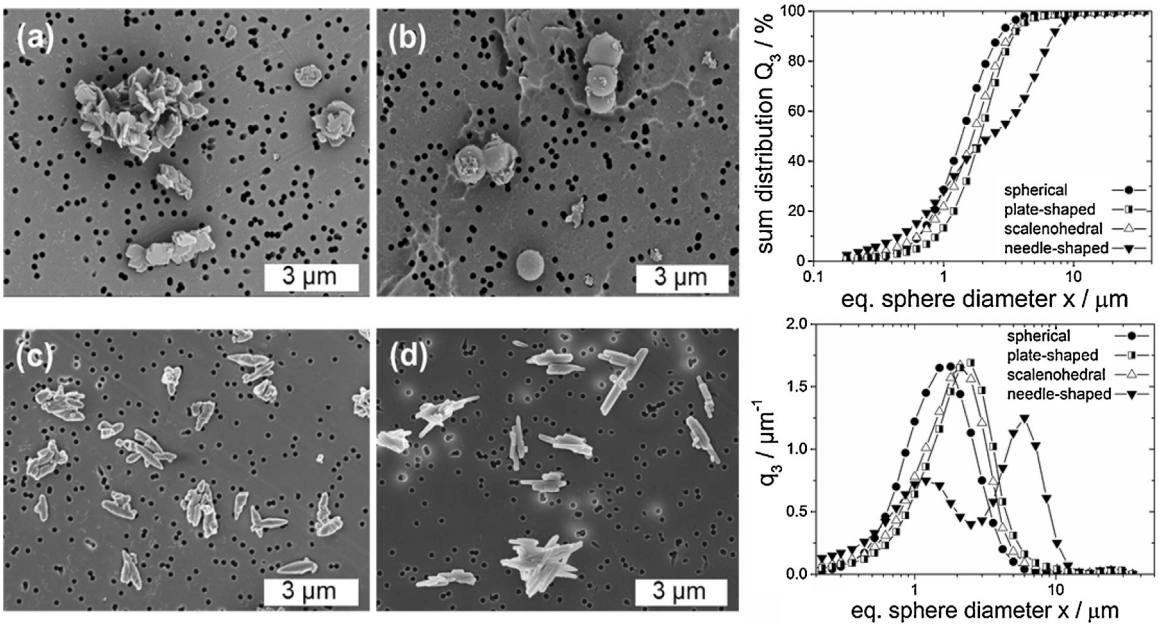

Fig. 1. Left: SEM images of the used PCC powders with different particle shapes: (a) plate-shaped, (b) spherical, (c) scalenohedral, (d) needle-shaped. Black dots in the background of the images result from sample preparation. Right: Particle size analysis of the used PCC powders. Differential particle size distribution q_3 and sum distribution Q_3 were determined through Fraunhofer diffraction.

Table 1
Material properties of used PCC powders. Crystal structure, density and specific surface are given by manufacturer.

product	**plate-shaped**	**spherical**	**scalenohedral**	**needle-shaped**
crystal structure	calcite	amorphous	calcite	aragonite
density (g/cm^3)	2.7	2.7–2.9	2.7	2.9
specific surface S_v (m^2/g)	17	8	9	10
aspect ratio r (−)	0.1 ± 0.0	1.0 ± 0.1	2.9 ± 0.8	7.9 ± 3.1
av. particle size $x_{50,3}$ (µm)	1.92 ± 0.0	1.4 ± 0.02	1.7 ± 0.02	2.2 ± 0.03

vance in this field since it allows for a demand-oriented adjustment of flow behavior and sedimentation stability without conventionally used organic additives (e.g. surfactants or thickeners) generally deteriorating electronic properties of the final dry film.

2. Experimental

Experiments were carried out using three different material systems: a set of four PCC samples with varying length over diameter ratio, i.e. aspect ratio r varying between 0.1 (plate-like) and 7.9 (needle-shaped), a pair of spherical and plate-like or flaky graphite samples, and two plate-shaped species of aluminum flakes with different aspect ratio. All these systems were characterized rheologically, additional structural investigations were performed on the PCC-based suspensions using confocal laser scanning microscopy (CLSM) and scanning electron microscopy (SEM).

2.1. Raw materials

Commercial grade precipitated calcium carbonate particles (PCC) were obtained from SCHAEFFER KALK GmbH & Co. KG (Diez, Germany). Four samples with different aspect ratio but also different crystal or amorphous structure were investigated, characteristic parameters are summarized in Table 1. Scanning electron microscopy (S-4500; Hitachi High-Technologies Europe GmbH, Krefeld, Germany) was used to determine the particle aspect ratio r via image analysis of at least 20 particles (Fig. 1). Fraunhofer diffraction (Helos H0309; Sympatec GmbH, Clausthal-Zellerfeld, Germany) was used to determine the equivalent sphere diameter distribution. A wet dispersing unit (Quixel; Sympatec GmbH) was used and particles were dispersed in ethanol, corresponding results are shown in Fig. 1. All PCC particles except the needle-shaped species show a similar equivalent sphere diameter distribution and average particle size. The apparent bimodality observed for the needle-shaped particles is a consequence of the large anisotropy [41,42]. Particle aspect ratio and average equivalent particle diameter are sufficient to describe the shape of all used particles, since they can be approximated as rotationally symmetric ellipsoids (oblate and prolate spheroids).

The bulk phase was paraffin oil (Carl Roth; Karlsruhe, Germany) with Newtonian flow behavior and a dynamic viscosity $\eta(20\,^\circ C) = 0.03$ Pa s. The nonionic wetting agent Polysorbat 20 (Tween20; Carl Roth) with HLB = 16.7 was used at a concentration of 0.2 vol% based on bulk phase to prevent unwanted agglomeration in the pure suspensions. The secondary liquid phase was pure water.

Two different, commercially available graphite powders were used as carbon material: SLP 30 (Imerys Graphite & Carbon; Bironico, Switzerland) contains plate-shaped particles with a density of $\rho = 2.27$ g/cm^3, an average equivalent particle diameter of $x_{50,3} = 15.6 \pm 0.1$ µm determined by Fraunhofer diffraction and a specific surface of 7 m^2/g (manufacturer information). SMGPA powder (China Steel Chemical Corporation; Kaohsiung, Taiwan) consists of spherical shaped particles with a density of $\rho = 2.21$ g/cm^3, an average equivalent particle diameter (volume median diameter) of $x_{50,3} = 7.7 \pm 0.1$ µm determined by Fraunhofer diffraction, and a specific surface of 2.2 m^2/g (manufacturer information). SEM-images (Fig. 2) of graphite particles were used to

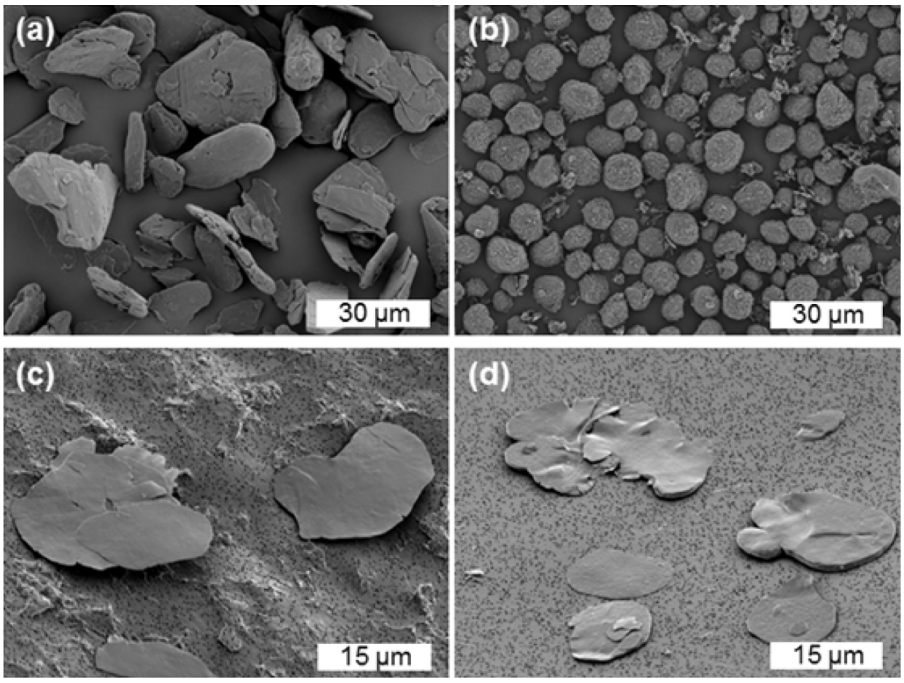

Fig. 2. SEM images of the graphite particles: (a) plate-shaped (aspect ratio $r = 0.15 \pm 0.04$), (b) spherical (aspect ratio $r = 1.2 \pm 0.1$), and of the aluminum particles with varying aspect ratio: (c) pigment 1, $r_1 = 0.013$, (d) pigment 2, $r_2 = 0.020$.

Table 2
Three-phase contact angle of all investigated material systems.

Material system	θ_{SB} (°)
calcite, paraffin oil (+Polysorbate 20), pure water	32 ± 4
aragonite, paraffin oil (+Polysorbate 20), pure water	79 ± 8
amorphous $CaCO_3$, paraffin oil (+Polysorbate 20), pure water	–
graphite, glycerol, octanol	78 ± 5
aluminum, paraffin oil, pure water	98 ± 14

determine aspect ratio r via image analysis of at least 20 particles (plate-shaped: $r = 0.15 \pm 0.04$, spherical: $r = 1.2 \pm 0.1$). Glycerol (Carl Roth; $\eta(20\,^{\circ}C) = 1.48$ Pa s) was used as bulk phase for this material system. 1-Octanol (purity > 99%; Merck Millipore, Darmstadt, Germany; $\eta(20\,^{\circ}C) = 0.009$ Pa s) was utilized as secondary liquid.

Aluminum particles (Schlenk Metallic Pigments GmbH; Roth, Germany) with two different aspect ratios (pigment 1: $r_1 = 0.013$, pigment 2: $r_2 = 0.020$; manufacturer information) were utilized. The particles exhibit the so-called silver dollar morphology, as shown by SEM micrographs in Fig. 2. Average equivalent particle diameter for both particle types is in the same range with $x_{50,3} = 16$–18 µm (manufacturer information). The particles were delivered dispersed in mineral spirit with a particle volume fraction of 30–35 vol%. The bulk phase for this material system was a mixture of paraffin oil (Carl Roth; $\eta(20\,^{\circ}C) = 0.03$ Pa s) and mineral spirit ($\eta(25\,^{\circ}C) \approx 0.001$ Pa s). Since mineral spirit is a mixture of paraffins, cycloparaffins and aromatic hydrocarbons it is completely miscible with paraffin oil. The mixing ratio of paraffin oil to mineral spirit was 1 : 0.3–0.5. The secondary liquid phase was pure water.

2.2. Sample preparation

Suspensions based on PCC particles were prepared by mixing the solid powder into the bulk phase with a high shear dissolver (diameter: 35 mm) at a speed of 1000 rpm for 15 min. Adding a small amount of the nonionic wetting agent Polysorbate 20 (0.2 vol% based on bulk phase) to the suspensions prevents unwanted agglomeration. This concentration guarantees a full coverage of the solid particles by the wetting agent (approximated with an average surface area per adsorbed Polysorbate 20 molecule on $CaCO_3$ of ~6 nm^2 [43]). The secondary fluid phase was added to the pure suspension using a high shear dissolver at a speed of 1000 rpm for 2 min, followed by a period of 2 min with reduced stirring speed at 500 rpm Graphite based suspensions were prepared by mixing the solid powder into glycerol using a high shear dissolver (diameter: 35 mm) at a speed of 1000 rpm for 10 min. Subsequently, secondary fluid was added to the suspension while stirring at 1000 rpm for 2 min. Afterwards the stirring speed was reduced to 500 rpm and mixing was continued for 5 min.

For preparation of the suspensions based on aluminum particles paraffin oil as bulk phase was added to the mineral spirit/particle mixture. The pure suspension was mixed with a high shear dissolver (diameter: 25 mm) at a speed of 1200 rpm for 10 min. Then the secondary fluid phase was added while stirring at a speed of 2000 rpm for 2 min. Afterwards the stirring speed was reduced to 800 rpm for 2 min.

2.3. Measurements

For contact angle measurements on $CaCO_3$ we used a rectangular calcite (2×2 cm) and a circular aragonite crystal (diameter 1 cm). The three-phase contact angle of the secondary fluid to the $CaCO_3$ was determined via the sessile drop method (OCA 15; Dataphysics) by applying the tangent method. Therefor small water drops were put on the $CaCO_3$ crystals surrounded by paraffin oil. The wetting agent Polysorbate 20 was added to the paraffin oil at a concentration of 0.2 vol%. The $CaCO_3$ crystals were stored in paraffin oil for ~10 min to allow for equilibrium adsorption of the wetting agent on the solid surface. Afterwards the secondary fluid drops were put on the $CaCO_3$ crystal; after another 10 min waiting time

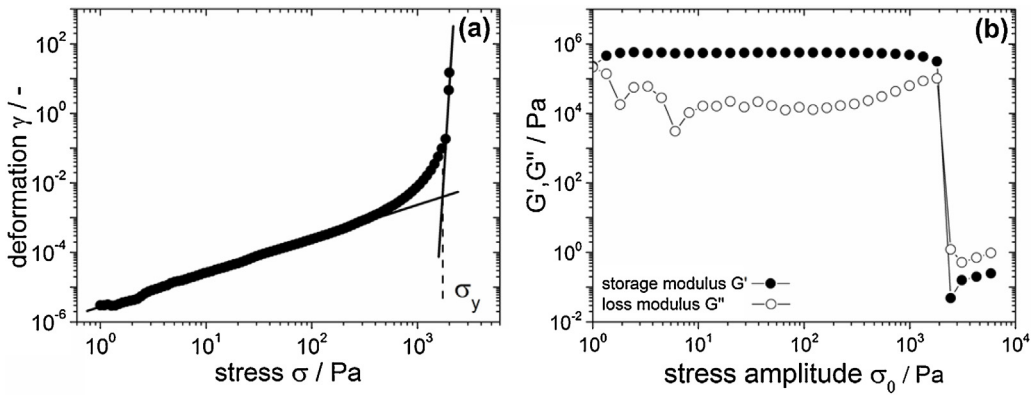

Fig. 3. Determination of yield stress of a three-phase suspension of plate-like PCC particles (ϕ_{solid} = 10 vol%, ϕ_{sec} = 4 vol%, bulk fluid = paraffin oil, secondary fluid = pure water). (a) Deformation vs. applied shear stress in stress ramp experiments performed using a vane geometry (σ = 0.1–4000 Pa, t_{dwell} = 10 s, vane dimensions: 22 × 10 mm). The yield stress is determined as the critical stress at the intersection of the tangents to the two branches of the curve. (b) Storage modulus G' and loss modulus G" as a function of applied stress amplitude in oscillatory shear experiments (ω = 1 s^{-1}). Two critical stresses are obtained: the stress $\sigma_{0,y}$ at which G' drops for more than one decade compared to the average value in the LVE regime and the stress $\sigma_{0,c}$ at which G' = G".

during which the wetting agent could diffuse into the secondary fluid drops the equilibrium contact angle was measured. Contact angles for the aluminum and the graphite system were determined via the same measuring procedure on an aluminum plate and a graphite plate, respectively.

Corresponding data are summarized in Table 2. The crystalline PCC systems and the graphite system exhibit three-phase contact angles below 90° and the corresponding value for the aluminum system is slightly above 90°. Data for amorphous PCC are not available since a macroscopic amorphous sample for θ_{SB} measurement was lacking.

Rheological properties of all suspensions were studied using rotational rheometry. Steady and oscillatory shear measurements for the suspensions based on PCC and aluminum particles were performed with the stress-controlled rheometer Haake Mars II (Thermo Scientific, Karlsruhe, Germany). All measurements were done at a temperature of T = 20 ± 0.5 °C. For steady yield stress measurements a vane geometry with an appropriate Searle cylinder (diameter of 20 mm after DIN 53019–1) was used [44]. Yield stress measurements were carried out by increasing shear stress stepwise in a shear stress range from σ = 0.1–4000 Pa, the dwell time at each stress level was set to 10 s. Oscillatory shear measurements were carried out using plate–plate geometry (diameter: 35 mm, gap height: 1.5 mm). To prevent wall slip of the suspensions a sandblasted lower steel plate (surface roughness ~1.2 μm) and a sandblasted upper titanium plate were used.

Yield stress measurements of the graphite suspensions were carried out by increasing shear stress stepwise in a shear stress range from σ = 0.08 Pa or 0.3 Pa to 80 Pa or 300 Pa respectively, using a stress-controlled rheometer RheoStress 1 (Thermo Scientific) with a plate-plate geometry (diameter: 35 mm, gap height: 1 mm). Each stress level was held constant for 5 s, total duration of a measurement run was 750 s.

Yield stress measurements for suspensions including aluminum flakes were carried out using a stress-controlled rheometer (Haake Mars II) by increasing shear stress stepwise in a shear stress range from σ = 0.1–1000 Pa, the dwell time at each stress level was set to 5 s.

For characterizing the microstructure of the PCC suspensions in the wet state a confocal microscope (TCS SP8; Leica Microsystems) with two solid state lasers (wave lengths λ = 488 nm and 552 nm) was used. Therefor the secondary liquid phase in the capillary suspensions was colored with a fluorescence dye (PromoFluor-488 Premium; PromoKine, Heidelberg, Germany), excitable at a laser wave length of 488 nm. The slight transparency of the suspensions

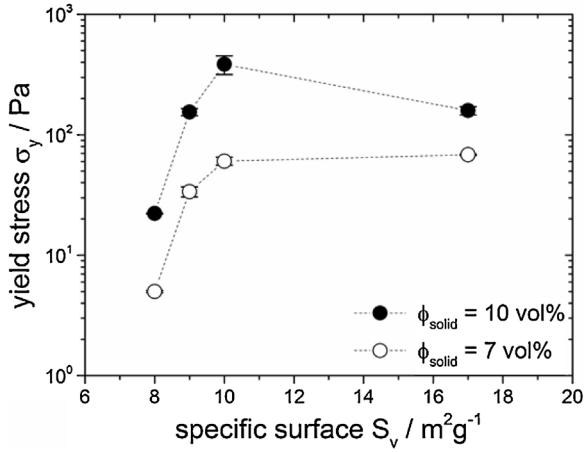

Fig. 4. Yield stress of suspensions consisting of PCC particles with varying particle shape dispersed in paraffin oil: spherical (S_v = 8 m^2/g), scalenohedral (S_v = 9 m^2/g), needle-shaped (S_v = 10 m^2/g), plate-shaped (S_v = 17 m^2/g).

allowed for taking images of the laser beam reflections in a sample depth of approximately 10 μm, due to using the reflection mode all interfaces in the sample were visible.

The microstructure of selected PCC suspensions was also characterized in the solid state. For this purpose suspensions were cast in spherical molds (diameter = 30 mm, height = 2 mm) dried and afterwards slightly sintered at a temperature of 500 °C for 1 h, and SEM micrographs (ESEM-mode at p = 70 Pa, Quanta 650 FEG; FEI, Hillsboro, USA) of fracture surfaces were taken.

3. Results and discussion

3.1. Determination of yield stress

A prominent characteristic feature of capillary suspensions is their high yield stress due to a strong sample-spanning particle network generated by capillary forces. Yield stress values for all three-phase suspensions consisting of PCC particles, paraffin oil and varying amounts of water as secondary liquid phase, were determined from steady and oscillatory shear experiments.

In steady shear stress was increased stepwise and the transition from solid to liquid-like behavior, i.e. the yield stress σ_y, was determined using the tangent method [45]. Typical deformation vs. stress data are shown in Fig. 3a, yield stress data provided below

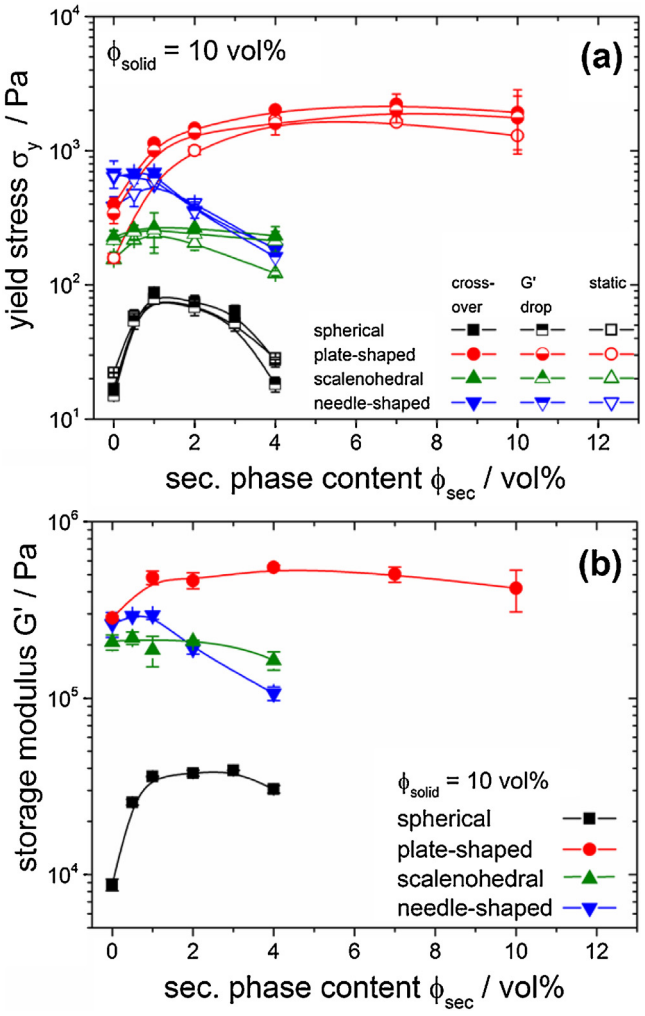

Fig. 5. (a) Yield stress σ_y vs. secondary phase content ϕ_{sec} for capillary suspensions consisting of PCC particles with varying particle shapes. Yield stress was determined with oscillatory shear experiments (crossover of G' and G" in amplitude sweep; drop of G') and with steady shear experiments (vane geometry). Error bars are the standard deviation calculated from at least three measurements. (b) Storage modulus G' vs. secondary phase content ϕ_{sec} for three-phase suspensions consisting of PCC particles with varying particle shapes. G' from amplitude sweep measurements at a frequency $\omega = 1\ s^{-1}$.

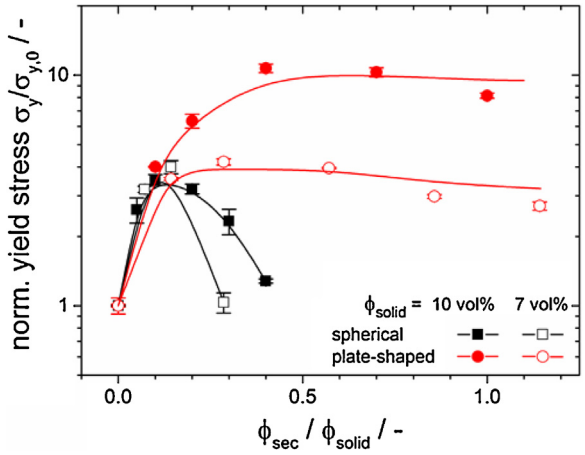

Fig. 6. Normalized yield stress $\sigma_y/\sigma_{y,0}$ vs. on particle solids fraction based secondary phase content ϕ_{sec}/ϕ_{solid}. Suspensions consist of spherical and plate-shaped PCC particles.

are average values and standard deviations were calculated from at least three measurements.

Oscillatory shear amplitude sweep measurements at constant frequency ω provide two characteristic stress values also related to the transition from solid to fluid-like behavior. Typical G' and G" vs. shear stress amplitude data are shown in Fig. 3b. G' is much larger than G" and an extended linear viscoelastic regime (LVE) is observed. A drop of G' for more than one decade compared to the LVE regime is defined as the criterion to determine the onset of non-linear response and the last data point before this drop occurs may also be treated as a yield value $\sigma_{0,y}$. The third yield value considered here, is $\sigma_{0,c}$ at the crossover of G' and G" (G' = G").

As will be shown below all three methods represent reliable and robust methods for determining yield stress of the three-phase suspensions investigated here without deviating much from each other.

3.2. Rheology of two-phase suspensions

Yield stress σ_y was determined for suspensions consisting of PCC particles with four different particle shapes (spherical, scalenohedral, needle-shaped, plate-shaped), dispersed in paraffin oil at two different solids concentrations ϕ_{solid} = 7 vol% and 10 vol%; no secondary liquid phase was added. Yield stress values σ_y as determined via steady shear rheometry are shown in Fig. 4 as a function of the specific surface of the PCC particles, given in Table 1. The high yield stress values found for these dilute suspensions indicate strong vdW attraction and corresponding formation of a sample spanning network.

The suspensions yield stress strongly varies with increasing specific surface S_V. Especially at $S_v < 10\ m^2/g$, small increases of S_v result in a strong increase in yield stress. However, it has to be considered that the change of specific surface also corresponds to a change in the particle shape here. This also has a significant influence on suspension rheology. The elongated, needle-shaped particles tend to have the highest yield stress at constant solids content although they do not show the highest specific surface. Similar results have been reported in literature for various other material systems [30,35].

3.3. Rheology of three-phase suspensions

Yield stress data for three phase suspensions based on PCC particles with different shape have been obtained from steady and oscillatory shear rheometry. Fig. 5a shows corresponding results obtained at a particle loading ϕ_{solid} = 10 vol% as a function of secondary fluid content. Within experimental uncertainity yield stress values obtained in different ways agree very well for the suspensions investigated here and especially they reveal the same trends regarding the effect of secondary fluid content on yield stress, i.e. network strength within the suspensions.

As shown in Fig. 5a only the three-phase suspensions including spherical and plate-shaped particles show the increase in yield stress upon addition of a secondary liquid phase typical for the so-called capillary suspensions with their strong capillary force controlled particle network [1]. The yield stress of suspensions consisting of plate-shaped particles increases by about a factor of ten while the spherical particles show an increase of about a factor of four compared to the yield stress of the respective pure suspensions $\sigma_{y,0}$. Whereas the yield stress of the plate-shaped particle suspensions exhibits an almost constant value for secondary fluid volume $2\% < \phi_{sec} < 10\%$, the yield stress of suspensions including spherical particles exhibits a pronounced maximum at $\phi_{sec} \approx 1$–2% and drops at higher ϕ_{sec} presumably due to spherical agglomeration [24]. Remarkably, elongated particles (scalenohedral and needle-shaped) do not show this behavior indicating that no capillary

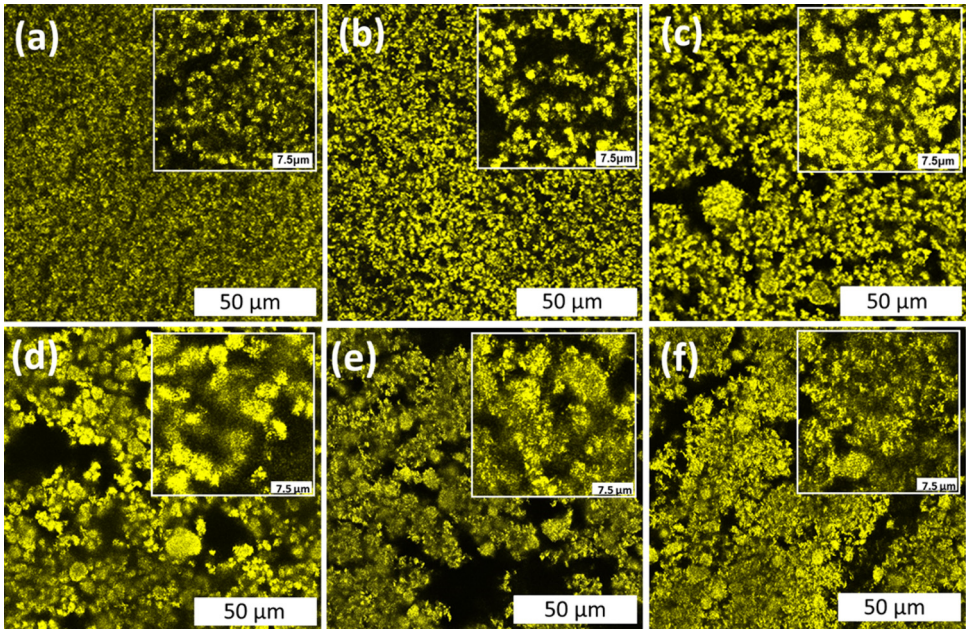

Fig. 7. CLSM images of two- and three-phase capillary suspensions consisting of PCC particles with different particle shapes (ϕ_{solid} = 10 vol%). Plate-shaped particles: (a) ϕ_{sec} = 0 vol%, (b) ϕ_{sec} = 4 vol%, (c) ϕ_{sec} = 10 vol%. Needle-shaped particles: (d) ϕ_{sec} = 0 vol%, (e) ϕ_{sec} = 1 vol%, (f) ϕ_{sec} = 4 vol%.

network is formed in these suspensions. An additional homogenization step in a ball mill did not change results significantly (data not shown here).

Characteristic differences regarding the effect of adding a secondary fluid to suspensions of different shaped particles showing up in yield stress measurements are further corroborated by storage modulus data. All suspensions show strong gel-like behavior with G' » G", but only when spherical or plate-shaped particles are included the addition of secondary fluid results in an increase in G' typical for capillary suspensions (Fig. 5b). A broad plateau of G' vs. ϕ_{sec} again is found for the plate-shaped particle suspensions, whereas a maximum in G' around $\phi_{sec} \approx 2\%$ as well as a drop in G' at higher ϕ_{sec} again indicating spherical agglomeration is found for the suspensions including spherical particles [24].

The pure two-phase suspension of the needle-shaped particles exhibits high σ_y and G' values indicating the existence of a strong particle network, but G' and σ_y do not increase upon addition of a secondary liquid instead both quantities quickly drop when the amount of secondary fluid is increased. So in this case the network cannot be reinforced by capillary forces, the drop in G' and σ_y instead may be due to spherical agglomeration.

An outstanding characteristic of the flake-shaped particles is the broad plateau observed in the σ_y and G' data. Obviously, these suspensions are able to incorporate large amounts of secondary liquid phase without change in rheological properties compared to spherical particles. This is directly evident from Fig. 6 where the relative increase in σ_y, i.e. $\sigma_y(\phi_{sec})/\sigma_y(\phi_{sec} = 0)$, is plotted vs. the ratio of secondary fluid volume ϕ_{sec} over particle volume fraction ϕ_{solid} for the plate-like and spherical particle suspensions at two different solids contents. For small ϕ_{sec}/ϕ_{solid} ratios, both types of suspensions exhibit a similar strong increase in yield stress. The suspensions with spherical particles then show a maximum in σ_y at $\phi_{sec}/\phi_{solid} \approx 0.1$ and for the plate-shaped particle suspensions σ_y further increases to reach its maximum at $\phi_{sec}/\phi_{solid} \approx 0.3$–$0.4$. When $\phi_{sec}/\phi_{solid} = 0.1$ is exceeded the normalized yield stress of suspensions including spherical particles drastically drops, and this decrease which is attributed to spherical agglomeration is more pronounced at lower particle loading since the lower number of aggregates can not provide a sample spanning network resulting in a measurable apparent yield stress. In contrast, the normalized yield stress of suspensions with plate-like particle remains almost constant up to $\phi_{sec}/\phi_{solid} \approx 1$, i.e. the network existing in the plate-like particle suspensions can accommodate an equal volume of secondary fluid and particles without change in σ_y, only at $\phi_{sec}/\phi_{solid} > 1$ a weak decrease in σ_y (and also G') occurs presumably due to the formation of dense aggregates. The oblate particles tend to absorb much more secondary liquid until the capillary bridges are supersaturated and spherical agglomeration sets in.

We assume these differences in rheological behavior are related to the shape of capillary bridges formed in suspensions of spherical and plate-like particles. Spherical particles in an ideal pendular state capillary suspension exhibit strongly localized, point-like contacts [2,20]. Increasing the liquid volume in pendular capillary bridges between two spherical particles leads to a maximum value of the resulting capillary force at a critical volume of the bridge [46]. Exceeding this limit, the curvature of the capillary bridge changes from concave to convex [9,47]. This results in a positive Laplace pressure in the capillary bridge and hence a reduced capillary force finally leading to the collapse of the capillary particle network. The bridges oversaturate and depending on secondary fluid volume and particle wetting properties a funicular network morphology may occur. At high enough ϕ_{sec} spherical agglomerates, consisting of large secondary liquid droplets including the suspended particles are formed [24,48]. In contrast, the curvature of the capillary bridge between two plate-shaped particles remains constant until the capillary bridge is completely filled. Capillary force increases monotonically with increasing capillary bridge volume [46] and the transition to spherical agglomeration and network collapse does not happen before the capillary bridges are completely filled.

Another factor affecting network strength and rheology of suspensions is the number of particle contacts, i.e. the coordination number. In dense packed granular matter oblate particles show a higher coordination number than spheres [49,50]. Accordingly, oblate particles should be able to build up more capillary bridges among each other than spherical particles. This should result not only in a higher yield stress of the pure suspension (see Fig. 4), but also in a stronger increase of the normalized yield stress of the three-phase suspension if enough secondary fluid is provided

as it seems to be the case for the plate-like particle suspensions investigated here at $\phi_{sec}/\phi_{solid} > 0.1$.

3.4. Microstructure in three-phase suspensions

Confocal laser scanning microscopy (CLSM) of wet suspensions and scanning electron microscopy of slightly sintered parts have been employed to gain insight into the microstructure of the investigated capillary suspensions consisting of PCC particles of different shapes. Samples with different secondary fluid content have been investigated and we attempt to relate the observed structural features to the rheological properties discussed above.

Fig. 7 shows CLSM images of wet suspensions of plate-shaped (Fig. 7a–c) and needle-shaped (Fig. 7d–f) particles with varying amounts of secondary liquid. Using the reflection mode of the confocal microscope all interfaces in the samples are visible. The microstructure of the suspensions with and even without secondary fluid (i.e. without fluorescence die) is directly observable. For suspensions of plate-like PCC particles three types of microstructure are observed depending on secondary fluid content: Without secondary fluid the particles are homogeneously distributed and only small textured areas indicate a vdW particle network (Fig. 7a). At secondary fluid content of 4 vol% the sample spanning particle network and the coarsening of the microstructure similar as previous observed for suspensions of spherical ceramic particles is apparent from the formation of flocs lancing through the suspension (Fig. 7b). Further increasing ϕ_{sec} results in a distinct heterogeneous suspension characterized by dense agglomerates, typically for supersaturated capillary suspensions [24]. In contrast, CLSM images of suspensions including needle-shaped PCC particles show similar microstructure irrespective of secondary fluid content: For all investigated ϕ_{sec} spherical clusters dominate the microstructures of the suspensions. Adding a secondary fluid to a pure suspension (Fig. 7e) changes the microstructure barely. The supersaturated suspension (Fig. 7f) is inhomogeneous and exhibits spherical agglomerates, which were even visible macroscopically.

SEM images of slightly sintered suspensions enables to visualize the arrangement of single particles in suspensions of plate-shaped and needle-shaped PCC particles at a higher resolution compared to CLSM. The gentle processing route for preparing the sintered parts [24] conserves the wet suspensions without major changes in microstructure. Fig. 8 shows the orientation of plate-shaped and needle-shaped particles in pure suspensions and corresponding three-phase suspensions. In pure suspensions the plate-like particles are well dispersed and only small aggregates consisting of randomly oriented flakes are observable (Fig. 8a). In the three-phase suspension the flakes are strongly aggregated to large clusters (Fig. 8b). Aggregates of prevalently parallel orientated flakes are predominant and this is attributed to the capillary forces acting between the particles. The microstructure of suspensions with needle-shaped PCC particles barely changes upon adding secondary fluid. Aggregates of spherical character are predominant in sintered parts of the two- and three-phase suspensions (Fig. 8c, d).

The structural features observed in wet and solid state can be well correlated to the rheological behavior discussed in chapters 3.1–3.3. Choosing three-phase suspensions with a σ_y and G' value in the plateau area, the plate-like particles show the typical structure formation in a capillary suspension, visible as small flocs in CLSM images. Supersaturating the capillary bridges leads to the formation of dense aggregates, resulting in the before observed decrease of σ_y and G'. The feature of plate-shaped particles to orient parallel in three-phase suspensions (schematically shown in Fig. 9a) favors the ability to incorporate large amounts of secondary liquid phase without change in microstructure and rheological properties. In contrast, the needle-shaped particles do not show a distinct structure formation in three-phase suspensions, agreeing

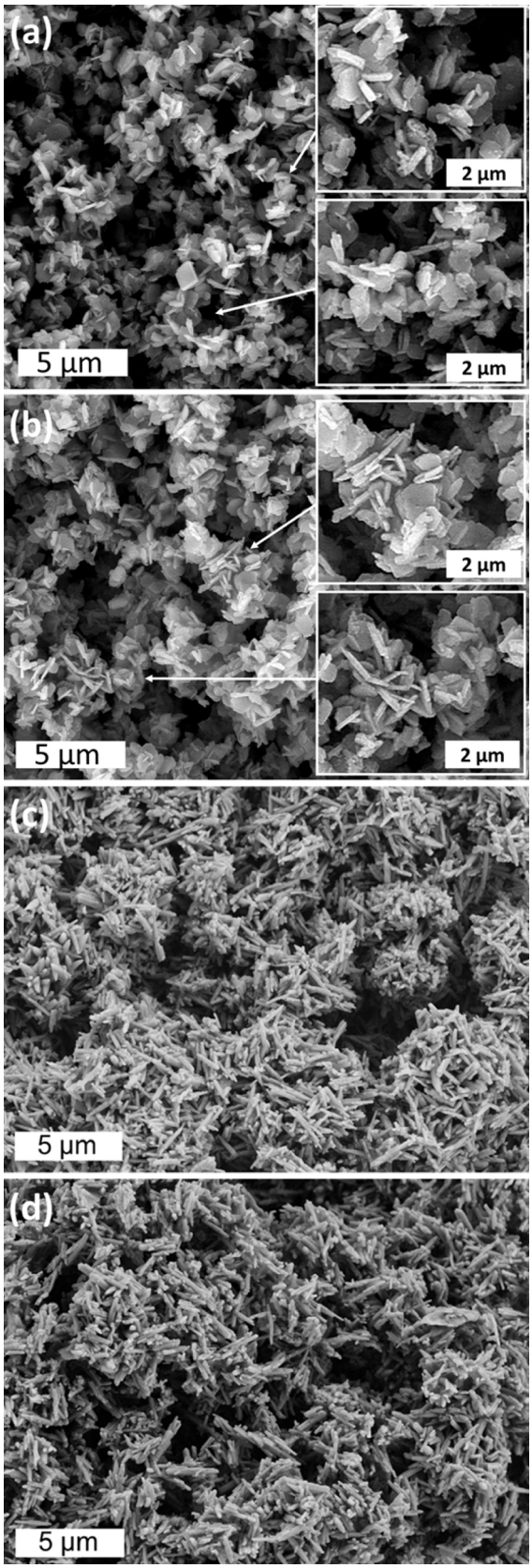

Fig. 8. SEM-images of slightly sintered suspensions, consisting of PCC particles. ϕ_{solid} = 10 vol%. Plate-shaped particles: (a) ϕ_{sec} = 0 vol%, (b) ϕ_{sec} = 4 vol%. Needle-shaped particles: (c) ϕ_{sec} = 0 vol%, (d) ϕ_{sec} = 1 vol%.

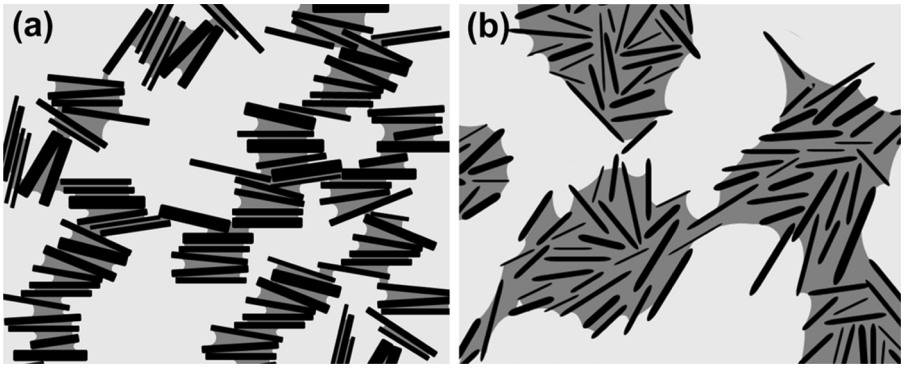

Fig. 9. Schematic images of three-phase suspensions with different particle shapes: (a) plate-shaped, (b) needle-shaped. Black: particles; dark grey: secondary fluid; light grey: bulk fluid.

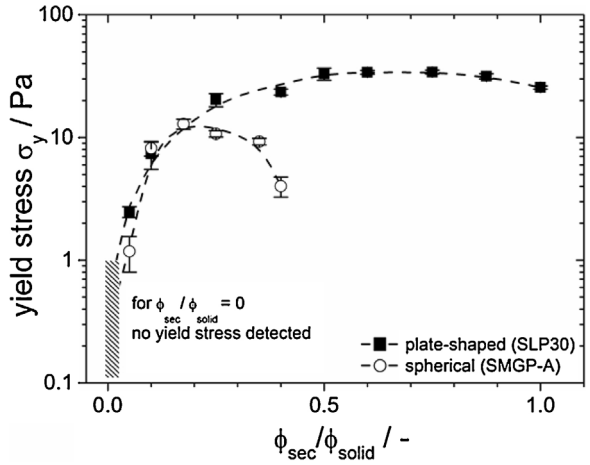

Fig. 10. Yield stress σ_y as function of ϕ_{sec}/ϕ_{solid} for graphite based three-phase suspensions using spherical and plate-shaped particles (ϕ_{solid} = 20 vol%). Bulk fluid: glycerol, secondary fluid: 1-octanol. The shaded area indicates that no reliable yield stress values can be determined at stresses below 1 Pa for the two phase graphite suspensions investigated here. The dashed lines are to guide the eye.

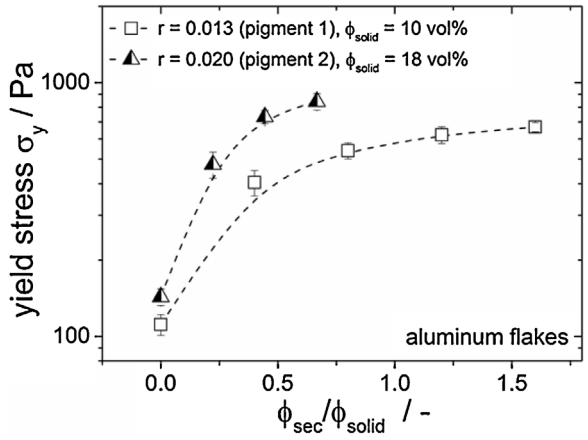

Fig. 11. Yield stress σ_y vs. ϕ_{sec}/ϕ_{solid} for suspensions consisting of aluminum flakes with varying aspect ratio. Bulk fluid: mixture of paraffin oil and mineral spirit. Secondary fluid: pure water.

with the results of rheological measurements. Spherical agglomerates (Fig. 9b) dominate the suspensions already at low secondary fluid content.

3.5. Three-phase suspensions for printed electronics

3.5.1. Graphite suspensions

Carbon based suspension systems are applied in various processes and fields of application, e.g. in the fabrication for Li-ion battery electrodes [51], supercapacitors [52] or gas-diffusion electrodes for Li-metal batteries and fuel cells [53–55]. Previously aqueous capillary suspensions containing spherical shaped graphite particles have been used to provide Li-ion battery anode pastes with tailor-made flow properties and superior coating behavior [19].

Here we employ spherical and plate-shaped graphite particles to create three-phase suspensions, using glycerol as bulk phase and 1-octanol as secondary liquid phase. Fig. 10 shows the yield stress σ_y as a function of ϕ_{sec}/ϕ_{solid} for three-phase suspensions of plate-shaped and spherical graphite particles. Without added secondary fluid the graphite suspensions do not show a yield stress. However, upon addition of secondary fluid a yield stress σ_y occurs and increases rapidly with increasing amount of secondary fluid for both systems. A maximum in σ_y is reached around ϕ_{sec}/ϕ_{solid} = 0.2–0.3 for the suspensions of spherical particles but σ_y decreases at higher amounts of secondary fluid due to spherical agglomeration. In contrast, the yield stress exhibits a broad plateau ranging from ϕ_{sec}/ϕ_{solid} = 0.25–1 for the three-phase suspensions of plate-shaped particles with no indication of spherical agglomeration. Qualitatively this is similar to what is found for PCC particles.

For both systems we assume the formation of a sample spanning network induced by capillary forces acting among suspended particles, i.e. formation of capillary suspensions.

3.5.2. Aluminum particles

Flake shaped Aluminum pigments are widely used in metallic automotive coatings to provide the desired gloss [56]. But they may also be used to print conductive fine lines or thin uniform layers in electronic applications. In both cases the particle aspect ratio has a strong impact of the final product properties.

Fig. 11 shows the yield stress vs. ϕ_{sec}/ϕ_{solid} for three-phase suspensions of oblate aluminum particles with two different aspect ratios (pigment 1: r = 0.013, pigment 2: r = 0.020). The solids content of both two-phase suspensions was chosen such that their respective yield stress values approximately match (ϕ_{solid} = 10 vol% for pigment 1 and ϕ_{solid} = 18 vol% for pigment 2).

In both cases the yield stress increases monotonically with increasing ratio of secondary fluid to solids volume fraction and an almost tenfold increase in σ_y is achieved. This is considered as a clear indication for the formation of a strong capillary force controlled particle network, i.e. capillary suspensions are created. The yield stress increases monotonically until a critical ratio ϕ_{sec}/ϕ_{solid} of 0.7 and 1.6, respectively, is reached. No macroscopically visible spherical agglomeration was observed up to this ϕ_{sec}/ϕ_{solid} ratio.

But at higher ϕ_{sec}/ϕ_{solid} values no homogeneous three-phase suspensions could be formed and the added secondary fluid could not be completely dispersed anymore. The capillary suspensions made from pigment 1 with the lower aspect ratio can accommodate more secondary fluid relative to the particle volume as revealed by the different critical ϕ_{sec}/ϕ_{solid} ratios. The increase in σ_y is more pronounced for the suspension made from pigment 2 with the higher aspect ratio. This might be due to the higher particle volume fraction leading to a different network structure [5].

No further interpretation can be provided on the basis of the currently available data a more quantitative investigation of the capillary suspension phenomenon for systems including anisotropic particles warrants further research work.

4. Conclusions

We investigated the rheological behavior and the microstructure of two- and three-phase suspensions consisting of precipitated calcium carbonate (PCC) particles with different shape (spherical, scalenohedral, needle-shaped, plate-shaped) as model systems in order to address the question how particle shape affects the formation of capillary force controlled sample-spanning networks upon addition of a secondary, immiscible fluid. Furthermore, we determined the rheological behavior of three-phase suspensions of graphite particles with different shapes and flake-shaped aluminum pigments with different aspect ratio, recognizing the particular technical importance of these particle systems.

At the investigated particle loading of 7 vol% and 10 vol% two-phase suspensions consisting of PCC particles show a strong gel-like behavior and yield stress strongly depends on specific surface and aspect ratio of the particles. Three-phase suspensions consisting of plate-like and spherical PCC particles show a drastic increase in σ_y and G' upon addition of the secondary fluid characteristic for capillary suspensions. For suspensions of spherical particles the rheological quantities strongly increase with increasing ϕ_{sec} to reach a maximum at $\phi_{sec}/\phi_{solid} \approx 0.1–0.2$ but they drastically drop at higher ϕ_{sec}/ϕ_{solid} and spherical agglomeration sets in. Suspensions of plate-like particles show a broad plateau in σ_y and G' at secondary fluid contents between $\phi_{sec}/\phi_{solid} = 0.2–1$ and only a weak decrease in σ_y at $\phi_{sec}/\phi_{solid} > 1$, presumably due to the formation of dense aggregates. The differences in rheological behavior of these differently shaped particles are assumed to be related to the shape of capillary bridges formed in the suspensions. Spherical particles show "point-like" bridges, which can be oversaturated already at low ϕ_{sec}. Capillary bridges between plate-like particles absorb large liquid volumes without supersaturating and collapsing.

Suspensions of elongated (scalenohedral, needle-shaped) PCC particles do not show a significant increase in σ_y and G' upon addition of secondary fluid, but these quantities strongly decrease for $\phi_{sec}/\phi_{solid} > 0.1$ due to the onset of spherical agglomeration.

CLSM and SEM imaging were utilized to investigate the microstructure of wet and slightly sintered PCC suspensions, respectively. For plate-shaped PCC particles formation of aggregates typical for three-phase so-called capillary suspensions and a preferential parallel orientation of the flakes was observed in the presence of the secondary, immiscible fluid. Suspensions of needle-shaped particles did not show significant differences in microstructure comparing two-phase with three-phase suspensions.

Finally, we investigated the effect of secondary fluid content on yield stress for graphite suspensions consisting of spherical and plate-shaped particles, and we observed similar behavior as for corresponding PCC suspensions, i.e. the plate shaped particles can accommodate much higher fractions of secondary fluid without spherical agglomeration than spherical particles. Investigating suspensions of flake-shaped aluminum particles we observed a monotonic increase in σ_y with increasing ϕ_{sec}/ϕ_{solid} ratio up to a critical value of this ratio beyond which homogeneous suspensions could not be prepared anymore. This increase in σ_y is more pronounced for the suspensions of particles with the higher aspect ratio but due to this higher aspect ratio the maximum relative amount of secondary fluid which can be accommodated inside the capillary bridges is lower in this case.

A deeper quantitative evaluation and investigation of capillary suspensions requires a broader data base including a series of particle systems with well-defined size, shape and surface properties varying in a broad parameter range. This has to be addressed in future work aiming at a prediction of important rheological quantities like yield stress and shear modulus as a function of particle volume fraction, size, shape and surface properties as well as type and amount of secondary fluid. In particular it will be important to determine the shape and volume of liquid bridges between plate-like particles and to evaluate how this affects structure and flow of the corresponding three-phase suspensions.

Acknowledgement

We would like to thank the SCHAEFFER KALK GmbH & Co. KG and the Schlenk Metallic Pigments GmbH for the donation of PCC particles and aluminum pigments as well as the smooth collaboration. The authors acknowledge the Competence-E project (KIT) for donation of graphite particles. Further thanks are given to Thomas Lebe for the work at the SEM-microscope and Klaus Hirsch for the particle size analysis. Frank Bossler is thanked for providing confocal laser microscope images and fruitful discussions. We acknowledge experimental support by Katrin Dyhr and Torsten Schick.

References

[1] E. Koos, N. Willenbacher, Capillary forces in suspension rheology, Science 331 (2011) 897–900.
[2] E. Koos, Capillary suspensions: particle networks formed through the capillary force, Curr. Opin. Colloid Interface Sci. 19 (2014) 575–584.
[3] S.S. Velankar, A non-equilibrium state diagram for liquid/fluid/particle mixtures, Soft Matter 11 (2015) 8393–8403.
[4] S.J. Heidlebaugh, T. Domenech, S.V. Iasella, S.S. Velankar, Aggregation and separation in ternary particle/oil/water systems with fully wettable particles, Langmuir 30 (2014) 63–74.
[5] E. Koos, N. Willenbacher, Particle configurations and gelation in capillary suspensions, Soft Matter. 8 (2012) 3988.
[6] S. Herminghaus, Dynamics of wet granular matter, Adv. Phys. 54 (2005) 221–261.
[7] C.D. Willett, M.J. Adams, S. a. Johnson, J.P.K. Seville, Capillary bridges between two spherical bodies, Langmuir 16 (2000) 9396–9405.
[8] H.J. Butt, Capillary forces: influence of roughness and heterogeneity, Langmuir 24 (2008) 4715–4721.
[9] D. Megias-Alguacil, L.J. Gauckler, Capillary forces between two solid spheres linked by a concave liquid bridge: regions of existence and forces mapping, AIChE J. 55 (2009) 1103–1109.
[10] T.P. Farmer, J.C. Bird, Asymmetric capillary bridges between contacting spheres, J. Colloid Interface Sci. 454 (2015) 192–199.
[11] E. Koos, J. Johannsmeier, L. Schwebler, N. Willenbacher, Tuning suspension rheology using capillary forces, Soft Matter. 8 (2012) 6620.
[12] H. Schubert, Capillary forces—modeling and application in particulate technology, Powder Technol. 37 (1984) 105–116.
[13] J. Dittmann, J. Maurath, B. Bitsch, N. Willenbacher, Highly porous materials with unique mechanical properties from smart capillary suspensions, Adv. Mater. (2015), http://dx.doi.org/10.1002/adma.201504910.
[14] E.B. Webb, C. a Koh, M.W. Liberatore, High pressure rheology of hydrate slurries formed from water-in- mineral oil emulsions, Ind. Eng. Chem. Res. 53 (2014) 6998–7007.
[15] S. Hoffmann, E. Koos, N. Willenbacher, Using capillary bridges to tune stability and flow behavior of food suspensions, Food Hydrocoll. 40 (2014) 44–52.
[16] S. Wollgarten, C. Yuce, E. Koos, N. Willenbacher, Tailoring flow behavior and texture of water based cocoa suspensions, Food Hydrocoll. 52 (2016) 167–174.
[17] Y. Zhang, M.C. Allen, R. Zhao, D.D. Deheyn, S.H. Behrens, J.C. Meredith, Capillary foams: stabilization and functionalization of porous liquids and solids, Langmuir 31 (2015) 2669–2676.

[18] Y. Zhang, J. Wu, H. Wang, J.C. Meredith, S.H. Behrens, Stabilization of liquid foams through the synergistic action of particles and an immiscible liquid, Angew. Chem. 126 (2014) 13603–13607.
[19] B. Bitsch, J. Dittmann, M. Schmitt, P. Scharfer, W. Schabel, N. Willenbacher, A novel slurry concept for the fabrication of lithium-ion battery electrodes with beneficial properties, J. Power Sources 265 (2014) 81–90.
[20] T. Domenech, S. Velankar, Capillary-driven percolating networks in ternary blends of immiscible polymers and silica particles, Rheol. Acta 53 (2014) 593–605.
[21] J. Xu, L. Chen, H. Choi, H. Konish, X. Li, Assembly of metals and nanoparticles into novel nanocomposite superstructures, Sci. Rep. 3 (2013) 1730.
[22] J. Dittmann, E. Koos, N. Willenbacher, Ceramic capillary suspensions: novel processing route for macroporous ceramic materials, J. Am. Ceram. Soc. 96 (2013) 391–397.
[23] J. Maurath, J. Dittmann, N. Schultz, N. Willenbacher, Fabrication of highly porous glass filters using capillary suspension processing, Sep. Purif. Technol. 149 (2015) 470–478.
[24] J. Dittmann, N. Willenbacher, Micro structural investigations and mechanical properties of macro porous ceramic materials from capillary suspensions, J. Am. Ceram. Soc. 97 (2014) 3787–3792.
[25] G.B. Jeffery, The motion of ellipsoidal particles immersed in a viscous fluid, Proc. R. Soc. A 102 (1922) 161–179.
[26] G.I. Taylor, The viscosity of a fluid containing small drops of another fluid, Proc. R. Soc. Lond. A 138 (1932) 41–48.
[27] J.M. Rallison, The effects of Brownian rotations in a dilute suspension of rigid particles of arbitrary shape, J. Fluid Mech. 84 (1978) 237–263.
[28] S. Haber, H. Brenner, Rheological properties of dilute suspensions of centrally symmetric Brownian particles at small shear rates, J. Colloid Interface Sci. 97 (1984) 496–514.
[29] H. Brenner, Rheology of a dilute suspension of axisymmetric Brownian particles, Int. J. Multiph. Flow. 1 (1974) 195–341.
[30] I. Santamaría-Holek, C.I. Mendoza, The rheology of concentrated suspensions of arbitrarily-shaped particles, J. Colloid Interface Sci. 346 (2010) 118–126.
[31] H. Giesekus, Disperse systems: dependence of rheological properties on the type of flow with implications for food rheology, in: R. Jowitt (Ed.), Phys. Prop. Foods, Applied Science Publishers, 1983, 2016.
[32] A.B.D. Brown, S.M. Clarke, P. Convert, A.R. Rennie, Orientational order in concentrated dispersions of plate-like kaolinite particles under shear, J. Rheol. 44 (2000) 221–233.
[33] S. Yamamoto, T. Matsuoka, Dynamic simulation of rod-like and plate-like particle dispersed systems, Comput. Mater. Sci. 14 (1999) 169–176.
[34] W. Pabst, E. Gregorová, C. Berthold, Particle shape and suspension rheology of short-fiber systems, J. Eur. Ceram. Soc. 26 (2006) 149–160.
[35] H.A. Barnes, J.F. Hutton, K. Walters, An Introduction to Rheology, 3rd ed., Elsevier Amsterdam, London, New York, Tokyo, 1993.
[36] D.A. Weitz, Packing in the spheres, Science. 303 (2004) 968–969.
[37] R.G. Larson, The Structure and Rheology of Complex Fluids, Oxford University Press, New York, USA, 1999.
[38] J. Mewis, N.J. Wagner, Colloidal Suspension Rheology, Cambridge University Press, New York, USA, 2012.
[39] R. Faddoul, N. Reverdy-Bruas, A. Blayo, Formulation and screen printing of water based conductive flake silver pastes onto green ceramic tapes for electronic applications, Mater. Sci. Eng. B. 177 (2012) 1053–1066.
[40] R. Faddoul, N. Reverdy-Bruas, A. Blayo, T. Haas, C. Zeilmann, Optimisation of silver paste for flexography printing on LTCC substrate, Microelectron. Reliab. 52 (2012) 1483–1491.
[41] H. Mühlenweg, E.D. Hirleman, Laser diffraction spectroscopy: influence of particle shape and a shape adaptation technique, Part. Part. Syst. Char. 15 (1998) 163–169.
[42] Z. Ma, H.G. Merkus, J. de Smet, C. Heffels, B. Scarlett, New developments in particle characterization by laser diffraction: size and shape, Powder Technol. 111 (2000) 66–78.
[43] E. Halder, D.K. Chattoraj, K.P. Das, Excess adsorption on hydrophobic and hydrophilic solid-liquid interfaces. Positive excess adsorption of non-ionic surfactant. Part 1, Indian J. Chem. Sect. A 45 (2006) 2591–2598.
[44] Q. Nguyen, D.V. Boger, Measuring the flow properties of yield stress fluids, Annu. Rev. Fluid Mech. 24 (1992) 47–88.
[45] R. Brummer, Rheology Essentials of Cosmetic and Food Emulsions, Springer Berlin-Heidelberg, 2006.
[46] Y.G. Tselishchev, V.A. Val'tsifer, Influence of the type of contact between particles joined by a liquid bridge on the capillary cohesive forces, Colloid J. Russ Acad. Sci. Kolloidn. Zhurnal. 65 (2003) 385–389.
[47] D. Megias-Alguacil, L.J. Gauckler, Analysis of the capillary forces between two small solid spheres binded by a convex liquid bridge, Powder Technol. 198 (2010) 211–218.
[48] T. Domenech, S.S. Velankar, On the rheology of pendular gels and morphological developments in paste-like ternary systems based on capillary attraction, Soft Matter 11 (2015) 1500–1516.
[49] S. Herminghaus, Wet Granular Matter: A Truly Complex Fluid, World Scientific, 2013.
[50] A. Donev, I. Cisse, D. Sachs, E. a Variano, F.H. Stillinger, R. Connelly, et al., Improving the density of jammed disordered packings using ellipsoids, Science 303 (2004) 990–993.
[51] J. Li, C. Daniel, D. Wood, Materials processing for lithium-ion batteries, J. Power Sources 196 (2011) 2452–2460.
[52] S. Faraji, F. Nasir, The development supercapacitor from activated carbon by electroless plating—A review, Renew. Sustain. Energy Rev. 42 (2015) 823–834.
[53] F. Cheng, J. Chen, Metal–air batteries: from oxygen reduction electrochemistry to cathode catalysts, Chem. Soc. Rev. 41 (2012) 2172.
[54] S. Litster, G. McLean, PEM fuel cell electrodes, J. Power Sources 130 (2004) 61–76.
[55] J.B. Xu, T.S. Zhao, Mesoporous carbon with uniquely combined electrochemical and mass transport characteristics for polymer electrolyte membrane fuel cells, RSC Adv. 3 (2012) 16–24.
[56] H. Harakawa, A. Kasari, A. Tominaga, M. Yatuba, The rheological properties of an aqueous acrylic dispersion suitable for automotive waterborne basecoats, Prog. Org. Coat. 34 (1997) 84–90.